Separation Science and Technology
Publication details, including instructions for authors and subscription information:
http://www.informaworld.com/smpp/title~content=t713708471

Mass Transfer Simulation of Carbon Dioxide Absorption in a Hollow-Fiber Membrane Contactor

S. Shirazian[a]; S. N. Ashrafizadeh[a]
[a] Research Laboratory for Advanced Separation Processes, Department of Chemical Engineering, Iran University of Science and Technology, Narmak, Tehran, Iran

Online publication date: 22 February 2010

To cite this Article Shirazian, S. and Ashrafizadeh, S. N.(2010) 'Mass Transfer Simulation of Carbon Dioxide Absorption in a Hollow-Fiber Membrane Contactor', Separation Science and Technology, 45: 4, 515 — 524
To link to this Article: DOI: 10.1080/01496390903530081
URL: http://dx.doi.org/10.1080/01496390903530081

Separation Science and Technology, 45: 515–524, 2010

ISSN: 0149-6395 print/1520-5754 online
DOI: 10.1080/01496390903530081

Taylor & Francis
Taylor & Francis Group

Mass Transfer Simulation of Carbon Dioxide Absorption in a Hollow-Fiber Membrane Contactor

S. Shirazian and S. N. Ashrafizadeh

Research Laboratory for Advanced Separation Processes, Department of Chemical Engineering, Iran University of Science and Technology, Narmak, Tehran, Iran

This paper presents the mass transfer simulation of the gas absorption process in a hollow-fiber membrane contactor by means of the finite element method. Theoretical mass transfer simulations were performed in order to describe the absorption of CO_2 by distilled water as well as aqueous solutions of diethanolamine. The simulations were focused on the behavior of gas and liquid phases in order to obtain the distribution of CO_2 and absorbent concentrations along the length of the membrane contactor. The effect of the operating parameters and membrane physical properties on the performance of the contactor was investigated. Validation of the applied simulation method, was made through comparing the calculated flux of CO_2 absorption with the experimental data reported in literature for a Celgard MiniModule. The obtained simulation results, which are in good agreement with the experimental values for different liquid velocities, reveal that the removal of CO_2 increases with porosity/tortuosity ratio and decreases with the inner diameter of the fibers. It is indicated that the proposed model well predicts the absorption mass transfer in the hollow-fiber membrane contactors.

Keywords gas separation; hollow fiber; mass transfer; membrane; simulation

INTRODUCTION

The expansion of industrial activities has caused the concentration of greenhouse gases to rise significantly in the atmosphere. This has contributed to global warming, which in turn has resulted in serious environmental problems (1). Carbon dioxide which is emitted from fossil fuel, natural and refinery off gases, and many other sources is representing about 80% of greenhouse gases. It has also been reported that half of the CO_2 emissions are produced by industry and power plants using petroleum-based fuels (2). It is thus important to separate CO_2 from gas mixtures to reach the carbon emission reduction targets set out by the Kyoto Agreement. Meanwhile, the CO_2 concentrations are about 3–5% in gas-fired power plants and 13–15% in coal plants (3).

The current carbon dioxide separation processes are based on physical and chemical processes including absorption, adsorption, cryogenic and membrane processes (4). The separation of CO_2 through ordinary processes experiences a number of shortcomings such as channeling, flooding, entraining, foaming, and also high capital and operating costs (4). As such, a large number of researchers have studied the possibilities of enhancing the efficiency of the latter processes to overcome the mentioned problems.

Recently, the gas-liquid hollow-fiber membrane contactors as gas absorption devices have become a subject of great interest. In these processes, the membrane contactor acts as a physical barrier between the two phases, i.e., gas and liquid. Due to a very high surface/volume ratio, the hollow-fiber membrane contactors (HFMCs) have a great potential for gas absorption. In addition, in gas-liquid hollow-fiber membrane contactors, the interfacial mass transfer area is relatively high, whereas the hydrophilic or hydrophobic nature of the membrane determines the position of the interface between the gas feed and the liquid absorbent (5).

A major part of the interest towards hollow fiber membrane contactors is due to their capability in setting a dispersion free contact. In addition, the velocities of both phases can be chosen independently, while neither flooding nor unloading problems arise (5). Figure 1 shows a parallel hollow-fiber membrane contactor.

Extensive research about the hollow-fiber membrane contactors has been conducted since Qi and Cussler first studied these devices (8). Using the polypropylene hollow-fiber membrane, Kreulen et al. (9) investigated the chemical absorption of CO_2 into water/glycerol liquid mixtures as absorbent. They studied the hollow-fiber membrane as a gas–liquid contactor in the case of both physical and chemical absorption. The separation of CO_2 from offshore gas using hollow-fiber membrane contactors was studied by Falk-Pederson and Dannstrom (10), who optimized the process with respect to size, weight, and costs. Several authors have studied the use of hollow-fiber membrane

Received 25 June 2009; accepted 22 November 2009.
Address correspondence to S. N. Ashrafizadeh, Research Laboratory for Advanced Separation Processes, Department of Chemical Engineering, Iran University of Science and Technology, Narmak, Tehran 16846, Iran. Tel.: +98-21-77240496; Fax: +98-21-77240495. E-mail: ashrafi@iust.ac.ir

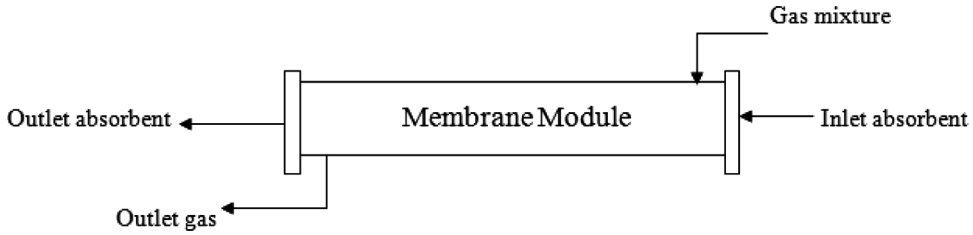

FIG. 1. A parallel flow hollow-fiber membrane contactor (6,7).

contactors for the absorption of CO_2 in a hydroxide solution (11), and the CO_2 removal through membrane using amino acid salts (12). Qi and Cussler (8) developed a theory for the operation of hollow-fiber membrane contactors, and calculated mass transfer coefficients in the liquid phase. They also obtained the overall mass transfer coefficients, including resistances in both liquid and membrane phases, and compared the performance of hollow-fibers with that of packed towers.

Some authors (13) investigated the separation of CO_2 and SO_2 from CO_2/N_2 and SO_2/air gas mixtures, using water as an absorbent in a parallel module employing microporous polypropylene hollow-fibers. A similar process has been recently studied by Dindore et al. (14) for gas–liquid contact in a hollow-fiber module. In both studies, the authors assumed negligible axial diffusion, which could be an erroneous assumption, especially for low gas velocities. Kim and Yang (15) investigated the separation of CO_2/N_2 mixtures using hollow-fiber membrane contactors theoretically and experimentally. Although there was an agreement between the model predictions with experimental results, the authors assumed a linear decrease of gas flow rate for the simulation purposes.

Al-Marzouqi et al. (16) developed a 2D mathematical model for simulation of CO_2 separation from CH_4 in a parallel hollow-fiber membrane module. They studied hollow-fiber membrane modules for physical absorption of carbon dioxide. Recently Shirazian et al. (17) studied the simulation of gas absorption in hollow-fiber membrane contactors for gas-liquid systems. They simulated these devices by using CFD techniques and validated simulation results with the experimental data for the physical absorption of CO_2 in pure water.

Hollow-fiber membranes are the most advantageous form of membranes used in the processes of gas separation. They can be produced by any method employed for the manufacture of chemical fibers, i.e., they can be spun from melt or half-melt or from a polymer solution. Melt-spinning is the most economical method of hollow-fiber membrane production. It is also a very ecological method, since no wastewater or harmful by-products are involved (18).

The main purpose of this study is to simulate CO_2 absorption through a hollow-fiber membrane contactor. The simulations are based on computational fluid dynamics of mass and momentum transfer in the liquid and gas phases. Other simulation studies on the membrane modules are only based on the mass transfer coefficients for gas and liquid phases and are not very accurate due to some simplifying assumptions such as neglecting axial diffusion in the mass transfer equations. In this work we solve the continuity equation along with the momentum equation in the membrane contactor in two dimensions. We also consider a reaction term in the continuity equation. The mass-transfer and momentum equations are solved by a numerical procedure based on the finite element method (FEM). The latter method has shown a reliable method for this process and geometry (19–23).

THEORY

To investigate the performance of hollow fiber membrane modules in the gas absorption process, a comprehensive two-dimensional mathematical model was used for the transport of carbon dioxide through hollow fiber membrane contactors (HFMCs). In this work we study the separation of CO_2 from CO_2/N_2 gas mixture using distilled water and aqueous diethanolamine (DEA) solutions as absorbents. The model was based on ''non-wetted mode'' in which the gas mixture filled the membrane pores for cocurrent gas–liquid contacts. Laminar parabolic velocity profile was used for the liquid flow in the tube side; whereas, the gas velocity in the shell side was characterized by solving the Navier-Stokes equation. Axial and radial diffusion were considered in the mass transfer equations. The model equations were solved by CFD method based on finite element method (FEM).

Mass Transfer Equations for the Membrane Contactor

The mass transfer model is used for a hollow fiber, as shown in Fig. 2. The liquid solvent flows with a fully developed laminar parabolic velocity profile inside the fiber and the gas mixture flows cocurrently through the shell side. Therefore, the membrane contactor consists of three sections: tube side, membrane, and shell side. The steady state two-dimensional material balances are carried out for all three sections.

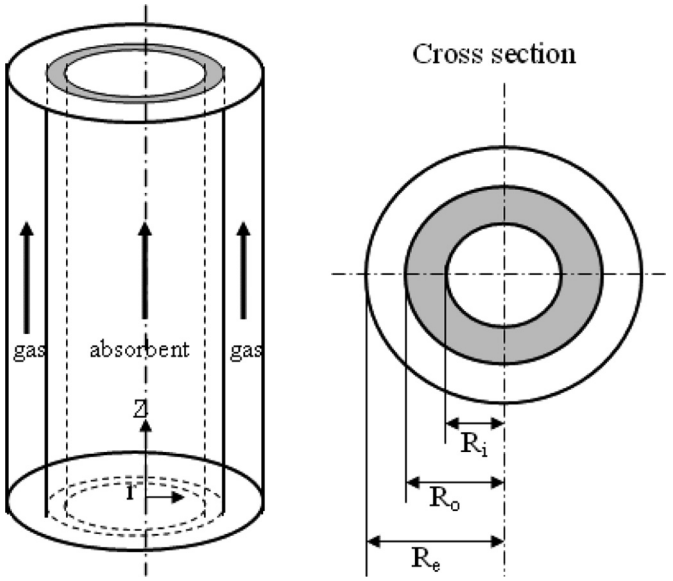

FIG. 2. Model domain and schematic diagram for a hollow-fiber (24).

The used assumptions were:

(1) steady state and isothermal conditions;
(2) fully developed parabolic liquid velocity profile in the hollow fiber;
(3) ideal gas behavior is imposed;
(4) the Henry's law is applicable for gas-liquid interface;
(5) Laminar flow for gas and liquid flow in the contactor.

The mass transfer equations for CO_2 and absorbent (i) are the convection-diffusion equations (25):

$$\frac{\partial C_i}{\partial t} + \nabla.(-D_i \nabla C_i + C_i V) - \Re_i = 0 \tag{1}$$

where $C_i, D_i, \Re_i, V$ and t are the concentration, diffusion coefficient, reaction rate of species i, velocity, and time, respectively. Equation 1 is a general form of convection-diffusion equation. In this study the steady-state condition is assumed for all equations, and thus the transient term is omitted in the proceeding equations.

For the tube side, the mass transfer equation (continuity equation) is:

$$D_{i-\text{tube}}\left[\frac{\partial^2 C_{i-\text{tube}}}{\partial r^2} + \frac{1}{r}\frac{\partial C_{i-\text{tube}}}{\partial r} + \frac{\partial^2 C_{i-\text{tube}}}{\partial z^2}\right] = V_{z-\text{tube}}\frac{\partial C_{i-\text{tube}}}{\partial z} - \Re_i \tag{2}$$

The chemical reaction occurs in the tube side, therefore continuity equation must be solved for the absorbent and CO_2 in the tube side.

The velocity distribution in the tube side is assumed to follow the Newtonian laminar flow (25):

$$V_{z-\text{tube}} = 2\overline{V}\left[1 - \left(\frac{r}{R_i}\right)^2\right] \tag{3}$$

For the shell side, the mass transfer equation is:

$$D_{\text{CO}_2-\text{shell}}\left[\frac{\partial^2 C_{\text{CO}_2-\text{shell}}}{\partial r^2} + \frac{1}{r}\frac{\partial C_{\text{CO}_2-\text{shell}}}{\partial r} + \frac{\partial^2 C_{\text{CO}_2-\text{shell}}}{\partial z^2}\right] = V_{z-\text{shell}}\frac{\partial C_{\text{CO}_2-\text{shell}}}{\partial z} \tag{4}$$

In the shell side, continuity equation must be solved only for CO_2 and there is no chemical reaction in the shell side.

The Navier-Stokes equations are used to characterize the shell side velocity. In the laminar flow, the Navier-Stokes equations apply (25):

$$\begin{aligned} &\rho\frac{\partial V}{\partial t} - \eta\nabla^2 V + \rho(V.\nabla)V + \nabla p = 0 \\ &\nabla.V = 0 \end{aligned} \tag{5}$$

where V, p, ρ, and η denote the velocity vector, pressure, density of the fluid, and the dynamic viscosity, respectively.

The gas flow in the shell side of the membrane contactor can be configured as fluid envelope around the fiber (Fig. 2) and there is no interaction between fibers (24). The dimension of the free surface can be estimated by Happel's free surface model (26):

$$R_e = \left(\frac{1}{1-\phi}\right)^{1/2} R_o \tag{6}$$

in which ϕ is the volume fraction of the void. It can be calculated as follows (26):

$$1 - \phi = \frac{nR_o^2}{R^2} \tag{7}$$

where n is the number of fibers and R is the module inner radius.

The steady-state continuity equation for the transport of CO_2 inside the membrane, which is considered to be due to diffusion alone, may be written as:

$$D_{\text{CO}_2-\text{membrane}}\left[\frac{\partial^2 C_{\text{CO}_2-\text{membrane}}}{\partial r^2} + \frac{1}{r}\frac{\partial C_{\text{CO}_2-\text{membrane}}}{\partial r} + \frac{\partial^2 C_{\text{CO}_2-\text{membrane}}}{\partial z^2}\right] = 0 \tag{8}$$

The boundary conditions are given in Table 1.

TABLE 1
Boundary conditions of mass transfer equations

Position	Tube	Membrane	Shell
$z = 0$ (Inlet)	$C_{CO_2} = 0$ $C_{absorbent} = C_{int}$	Insulated*	$C_{CO_2} = C_0$ $C_{absorbent} = 0$
$z = L$ (Outlet)	Convective flux	Insulated*	Convective flux
$r = R_i$	$C_{CO_2} = C_{CO_2\text{-membrane}} \times m$ $\frac{\partial C_{absorbent}}{\partial r} = 0$ (non-wetted)	$C_{CO_2} = C_{CO_2\text{-tube}}/m$	—
$r = R_o$	—	$C = C_{CO_2\text{-shell}}$	$C = C_{CO_2\text{-membrane}}$
$r = R_e$	—	—	$\frac{\partial C_i}{\partial r} = 0$ (symmetry)

*It is assumed that there is no mass transfer at both edges of the fibers.

where m is solubility of CO_2 in the solvent. Diffusion mechanism ($V = 0$) is assumed for mass transfer of CO_2 within the membrane. The chemical reaction only occurs in the tube side. For other sections the reaction term is zero ($\Re = 0$).

Reaction Rate for CO_2 Absorption into DEA Aqueous Solution

Zwitterion mechanism has been commonly accepted as the reaction mechanism between CO_2 and primary or secondary amines (24). Originally proposed by Caplow (27) and reintroduced by Danckwerts (28), the mechanism can be represented in two steps as follows (24,27,28):

$$CO_2 + R_1R_2NH \overset{k_1}{\longleftrightarrow} R_1R_2NH^+COO^- \quad (9)$$

$$R_1R_2NH^+COO^- + B \xrightarrow{k_b} R_1R_2NCOO^- + BH^+ \quad (10)$$

In the first step, CO_2 reacts with DEA to form zwitterions, which are deprotonated by the bases denoted as B in the solution in the second step. In the aqueous DEA solution, the bases are DEA, water and hydroxyl ions (24,29).

Based on the assumption of quasi-steady-state condition for the zwitterions concentration, the rate of CO_2 reaction with DEA was derived as (30–34):

$$\Re_i = \frac{[DEA][CO_2]}{\frac{1}{k_1} + \frac{1}{(k_1 k_{H_2O}/k_{-1})[H_2O] + (k_1 k_{OH^{-1}}/k^{-1})[OH^{-1}] + (k_1 k_{DEA}/k_{-1})[DEA]}} \quad (11)$$

where the effect of hydroxyl ion (OH^{-1}) can be neglected without causing a substantial loss of accuracy (30) and the kinetic parameters are listed in Table 2.

Physical Properties and Numerical Solution of Equations

The dimensions of the membrane contactor used for the numerical simulation are the same as those in Ref. 24. The numerical simulations are realized for a large range of inlet flow rates at the tube and shell sides, which can be obtained with these membrane devices. A range of inlet flow rates at the shell and tube sides from 20 to 600 mL/min were chosen and used for simulation. The density and the viscosity data for gas phase are those of nitrogen because of low concentration of carbon dioxide in the gas mixture. The inlet concentration of CO_2 in the gas phase for all of the cases is 10 vol%. Two typical values of diffusion coefficients are used in the simulation, i.e., the carbon dioxide in the nitrogen and carbon dioxide in the absorbent. The physical properties are summarized in the Table 3.

The model equations related to tube side, membrane, and shell side with the appropriate boundary conditions were solved using COMSOL Multiphysics software, which uses the finite element method (FEM) for numerical solution of differential equations. The finite element analysis is combined with adaptive meshing and error control using stationary nonlinear numerical solver. The nonlinear solver uses an affine invariant form of the damped Newton method. The use of FEM allows mass conservation in the domain; therefore "numerical loss" of mass in the computational domain is not a major concern. The applicability, validity, and robustness of the FEM method for the kind of domain encountered in the present work have been demonstrated by a number of previous authors (19–23).

An IBM-PC-Pentium4 (CPU speed is 2800 MHz) was used to solve the set of equations. The computational time for solving the set of equations was about 33 minutes.

Figure 3 shows a segment of the mesh used to determine the gas transport behavior in hollow-fiber membrane

TABLE 2
Kinetic parameters of reaction between CO_2 and DEA at 298 K (34)

DEA concentration ($mol\,m^{-3}$)	150–2500
k_1 ($m^3\,mol^{-1}\,s^{-1}$)	2.375
$\frac{k_1 k_{H_2O}}{k_{-1}}$ ($m^6\,mol^{-2}\,s^{-1}$)	2.2E-6
$\frac{k_1 k_{DEA}}{k_{-1}}$ ($m^6\,mol^{-2}\,s^{-1}$)	4.37E-4

TABLE 3
Physical properties of CO_2 in water and aqueous solution of 2 M DEA at 298 K (24)

Absorbent	Component	Solubility (mol/mol)	Diffusivity (m^2/s)
Water	CO_2	0.833	1.92E-9
Aqueous solution of 2 M DEA	CO_2	0.765	1.047E-9
Aqueous solution of 2 M DEA	DEA	—	4.967E-10

contactor (HFMC). It should be pointed out that the COMSOL mesh generator creates triangular meshes that are isotropic in size. A large number of elements are then created with scaling. A scaling factor of 100 (the fiber length is 100 mm) has been employed in z-direction due to a large difference between r and z. COMSOL automatically scales back the geometry after meshing. This generates an anisotropic mesh around 1235 elements. Adaptive mesh refinement in COMSOL, which generates the best and minimal meshes, was used to mesh the contactor geometry.

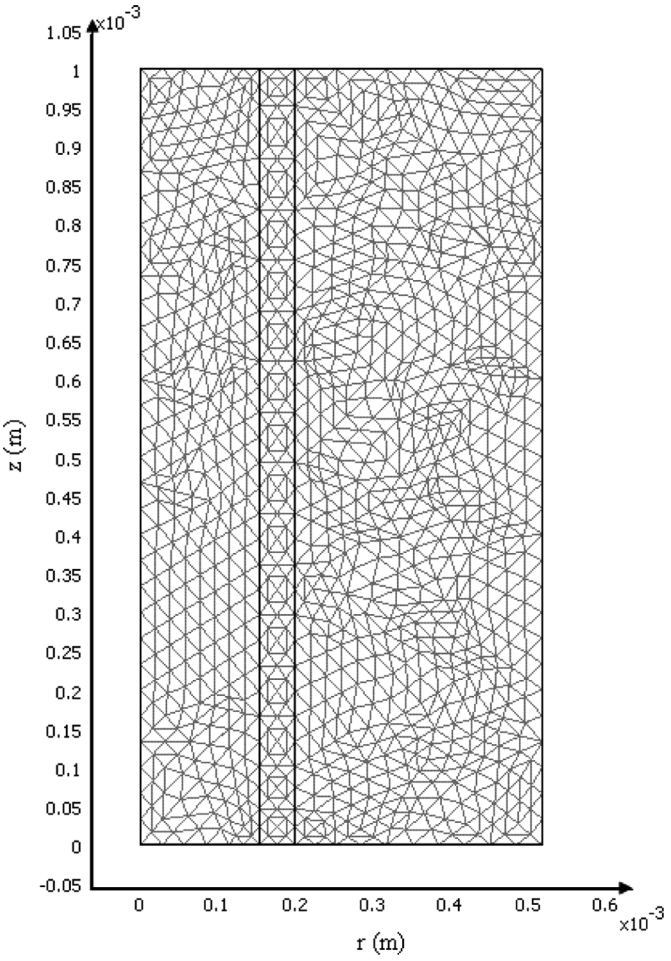

FIG. 3. Magnified segments of the mesh used in the numerical simulation. There are 1235 elements in total for the whole HFMC domain. z-direction scale factor = 100. The three domains from left to right are the tube side, membrane, and shell side, respectively.

RESULTS AND DISCUSSIONS

Effect of Liquid Phase Velocity on the Mass Transfer of CO_2

The percentage removal of CO_2 can be calculated from Eq. 12:

$$\text{CO}_2\ \text{Removal}(\%) = 100 \times \frac{(Q \times C)_{inlet} - (Q \times C)_{Outlet}}{(Q \times C)_{inlet}} = 100 \times \left(1 - \frac{C_{out}}{C_{in}}\right) \quad (12)$$

Where Q and C are the volumetric flow rate and concentration, respectively. C_{out} is calculated by integrating the local concentration at outlet of shell side (z =L):

$$C_{out} = \frac{\int\int_{Z=L} C(r)dA}{\int\int_{Z=L} dA} \quad (13)$$

The change in volumetric flow rate is assumed to be negligible and thus % CO_2 removal can be approximated by Eq. 12.

To calculate the Reynolds number, velocity of the liquid phase in the hollow-fibers is required. The velocity of the liquid phase can be obtained from Eq. 14:

$$\overline{V}_{tube} = \frac{Q_l}{n\pi(R_i)^2} \quad (14)$$

Therefore, the Reynolds number for the liquid phase is calculated through Eq. 15:

$$\text{Re}_l = \frac{2 \times \overline{V}_{tube} \times R_i}{\nu_w} \quad (15)$$

where ν_w is kinematic viscosity of the liquid phase. For simulation purposes, the kinematic viscosity of DEA solution is assumed equal to that of the pure water.

Figures 4 and 5 indicate the CO_2 outlet concentration and the Removal of CO_2 versus Reynolds number. The figures also show that the Reynolds numbers are very low. Therefore, the hypothesis of laminar flow is really rational for these cases.

In Fig. 4, the CO_2 concentration in the gas phase outlet stream is plotted as a function of the liquid phase Reynolds number for two absorbents. Figure 5 shows the percentage

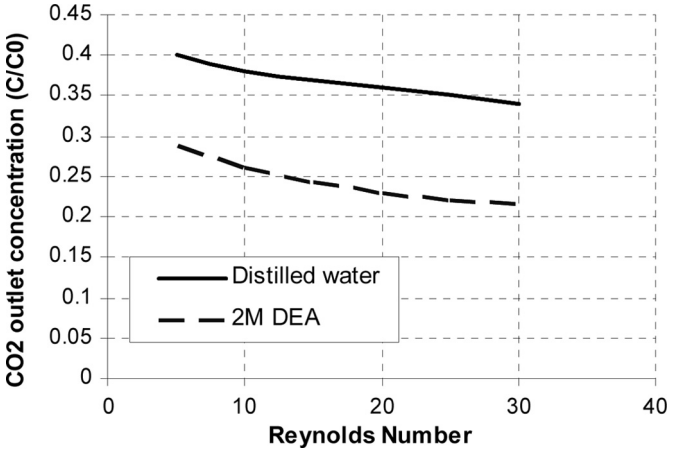

FIG. 4. CO_2 outlet concentration in the gas phase vs. liquid phase Reynolds number. Gas pressure = 121.3 kPa; temperature = 298 K; gas flow rate = 100 mL/min; $n = 100$; $R = 2$ cm.

removal of CO_2 as a function of the liquid phase Reynolds number. As it is shown, by increasing the Reynolds number, the mass transfer rate of carbon dioxide into the liquid phase is increased. The latter is due to the increase in concentration gradients of CO_2 and absorbent in the liquid phase. Therefore, the CO_2 concentration in the gas phase outlet stream decreases (Fig. 4); i.e., the removal of CO_2 increases (Fig. 5).

The behavior of CO_2 absorption in both DEA aqueous solution and water is also illustrated in Figs. 4 and 5. Addition of DEA into the water increases the removal of CO_2 because of the reaction of DEA with CO_2 which increases the mass transfer rate of CO_2 through the membrane. As a result, the CO_2 outlet concentration in the gas phase decreases and the removal of CO_2 improves.

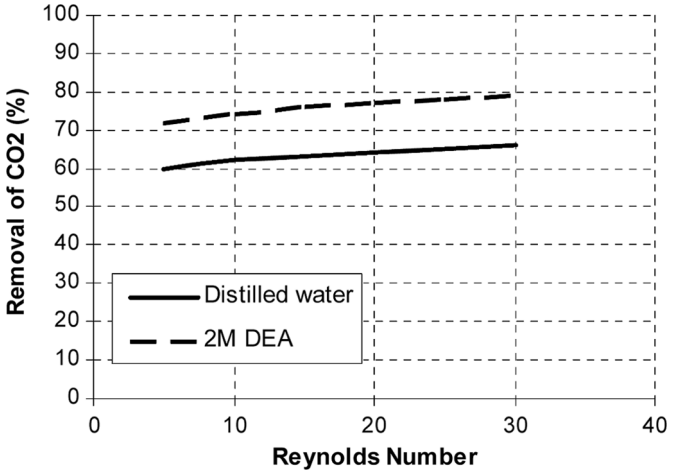

FIG. 5. Removal of CO_2 (%) vs. liquid phase Reynolds number. Gas pressure = 121.3 kPa; temperature = 298 K; gas flow rate = 100 mL/min; $n = 100$; $R = 2$ cm.

Effect of Gas Velocity on the CO_2 Removal

The percentage removal of CO_2 in the gas phase along the length of membrane contactor for different values of gas flow rates (the effect of convection term) is presented in Fig. 6. As expected, the increase in the gas flow rate reduces the residence time of the gas phase in the membrane contactor, which in turn reduces the removal rate of CO_2 in the contactor. The percentage removal of CO_2 decreases from 52% to 47% when the gas flow rate in the membrane contactor changes from 100 ml/min to 500 ml/min. Also, Fig. 6 indicates that the gas flow rate dose not greatly affect the CO_2 removal in the membrane contactor.

Concentration Distribution of DEA in the Membrane Contactor

Figure 7 represents the dimensionless concentration of DEA versus dimensionless axial distance (Z/L) along the membrane contactor. The simulation results show that the concentration of DEA decreases as the axial distance increases. It can be seen from the figure that depletion of DEA is very large along the membrane length. This indicates the concentration gradient of DEA is large due to the large reaction coefficient of DEA with CO_2. Consequentially, the consumption of DEA is large in the membrane contactor.

Effect of Membrane Physical Properties

Effect of Porosity-to-Tortuosity Ratio

A variation of the porosity-to-tortuosity ratio between 0.05 and 0.50 has been considered in the simulations to investigate the effect of this parameter on the mass transfer of CO_2. These ratio values correspond to those of current porous membranes which have porosity between 0.15 and 0.75 and tortuosity between 2 and 3 (values reported by

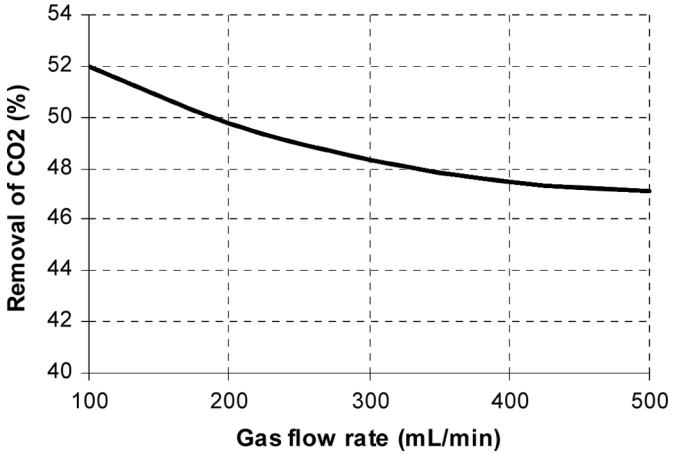

FIG. 6. Removal of CO_2 (%) vs. gas flow rate. Gas pressure = 121.3 kPa; temperature = 298 K; liquid flow rate = 100 mL/min; $n = 100$; $R = 2$ cm.

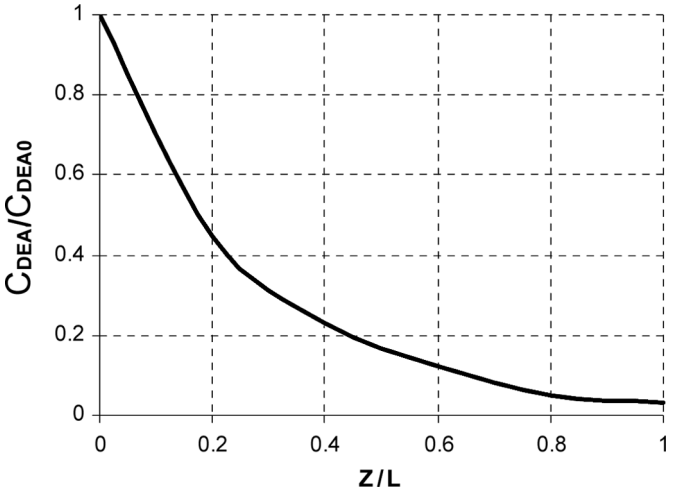

FIG. 7. Dimensionless concentration of DEA vs. dimensionless axial distance. Gas pressure = 121.3 kPa; temperature = 298 K; gas flow rate = liquid flow rate = 50 mL/min; $r/R_i = 0.8$; $C_{DEA0} = 2$ M.

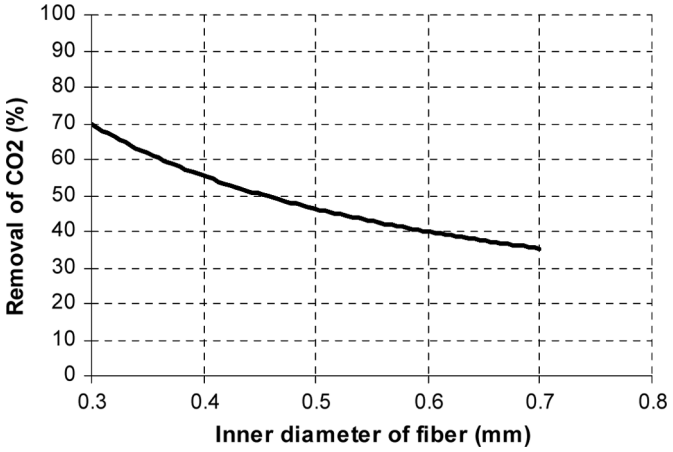

FIG. 9. Removal of CO_2 (%) vs. inner diameter of the fibers. Gas pressure = 121.3 kPa; temperature = 298 K; gas flow rate = liquid flow rate = 100 mL/min; $C_{DEA0} = 2$ M.

Gabelman and Hwang (4)). Figure 8 represents the effect of the porosity-to-tortuosity ratio on the removal of CO_2. The removal of CO_2 has grown about 2.6 times when the latter ratio increases from 0.05 to 0.50. The effective diffusion coefficient ($D_{CO_2\text{-membrane}}$) of the membrane is calculated through the porosity and tortuosity of the membrane (eq. 16), which are provided by the membrane manufacturer (4):

$$D_{CO_2-\text{membrane}} = D_{CO_2-\text{shell}}\left(\frac{\varepsilon}{\tau}\right) \tag{16}$$

As it can be seen from Eq. 16, the effective diffusion coefficient is a function of porosity and tortuosity of membrane. As the porosity/tortuosity ratio increases, the membrane diffusivity and thus the mass transfer of CO_2 through the membrane increases; i.e., the removal of CO_2 increases. Indeed, when the porosity/tortuosity ratio increases, the membrane mass transfer resistance decreases. Therefore, the total resistance to the mass transfer of CO_2 becomes lower.

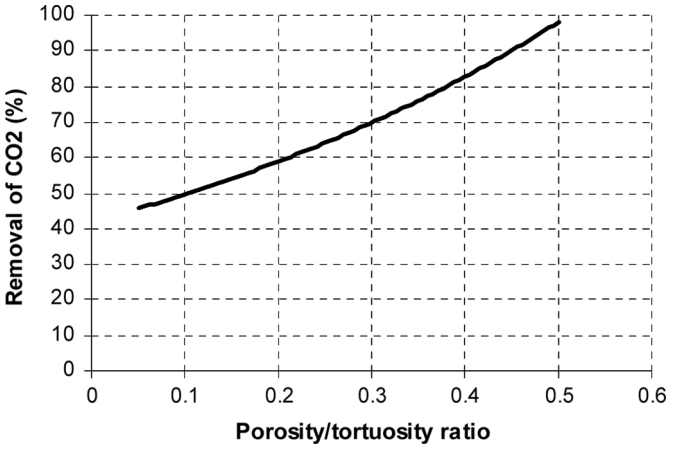

FIG. 8. Removal of CO_2 (%) vs. porosity/tortuosity ratio. Gas pressure = 121.3 kPa; temperature = 298 K; gas flow rate = liquid flow rate = 100 mL/min; $C_{DEA0} = 2$ M.

Effect of Geometrical Parameters of the Hollow Fibers

The influence of the inner diameter of the hollow fibers was investigated in the simulations. In order to maintain the thickness of the membrane constant, the inner and outer diameter of the hollow fibers were varied simultaneously. It is important to note here that the flow rate of gas and liquid phases were kept constant. This means that when the inner diameter increases, the velocity of the liquid phase decreases and velocity of gas phase increases. In fact the variation of the diameter, keeping the thickness constant, will lead to a change of the mass transfer area, of the hydrodynamics on both sides of the membrane, and subsequently the mass transfer resistances. The inner diameter of the fibers has been increased in a range from 0.3 to 0.7 mm, whereas the thickness of the membrane was kept at 0.2 mm. The influence of this parameter on the removal of CO_2 is presented in Fig. 9. As it is shown, the removal of CO_2 has decreased substantially, as the inner diameter increases.

Increasing the inner diameter of the fibers at a constant volumetric flow rate, leads to a reduction in the liquid velocity, which is flowing inside the fibers. At the same time, the gas phase velocity is increased and decay in the residence time of the gas phase, which is flowing in the shell side, occurs. Both phenomena contribute to the removal decrease.

MODEL VALIDATION

In order to verify the mass transfer model used for simulation, the simulation results were compared with the experimental values reported by Zhang et al. (24). They

TABLE 4
Module parameters of Zhang et al.'s experimental set up (24)

Module length (mm)	188
Fiber o.d. (μm)	300
Fiber i.d. (μm)	220
Fiber length (mm)	113
Number of fibers	1100
Pore size (μm)	0.04
Porosity	0.40
Contact area (m^2)	0.09

reported experimental results for the separation of CO_2 from CO_2/N_2 gas mixture by a hollow membrane module. In this section we compare the absorption flux of CO_2 calculated by simulation with the experimental values of Zhang et al. (24) to verify the simulation results. They used a Celgard microporous hollow-fiber MiniModule 0.75×5, which was provided by Celgard Inc., as a contactor in their study. The hollow fibers in the module were X-50 type and made of polypropylene. The characteristics of the membrane contactor are listed in Table 4.

The experimental setup is schematically presented in Fig. 10. CO_2/N_2 gas mixture with a volume ratio of 20/80 was used as the feed gas while the N_2 saturated distilled water or aqueous 2 M DEA solution was used as the absorbent. In their study, the gas always passed through the shell side and the liquid flowed cocurrently through the lumen side of the hollow fibers (24).

The effect of liquid velocity on the flux of CO_2 is presented in Fig. 11. As shown in this figure, the results of the simulation match quite well with the experimental data. In the low regime of liquid velocity ($U_L < 0.05\,m/s$), the flux of CO_2 absorption increases with the liquid velocity. This is perhaps due to the significant consumption of active amines in the solution. With a further increase of the liquid velocity, the supply of the active amines is accelerated and the depletion could be effectively mitigated (24). Thus in the regime where the liquid velocity is relatively high ($U_L > 0.1\,m/s$), the CO_2 flux is almost not affected by the liquid velocity. From the viewpoint of applications, the high velocity regime is ideally suitable for the operation of membrane contactors (24).

The CO_2 mass transfer flux can be obtained from Eq. (17):

$$J_{CO_2} = \frac{(Q_{in} \times C_{in} - Q_{out} \times C_{out})}{S} \tag{17}$$

where J_{CO_2} is the mass transfer flux of CO_2, $mol/(m^2s)$; Q_{in} and Q_{out} are the gas flow rates at the inlet and the outlet, m^3/s, respectively; C_{in} and C_{out} are CO_2 volumetric concentrations in the gas phase at the inlet and outlet, mol/m^3, respectively; S is the gas-liquid interfacial area, m^2.

There are little differences between experimental data and simulation results. Equation (17) is used for the calculation of the CO_2 absorption flux. It is assumed that the gas

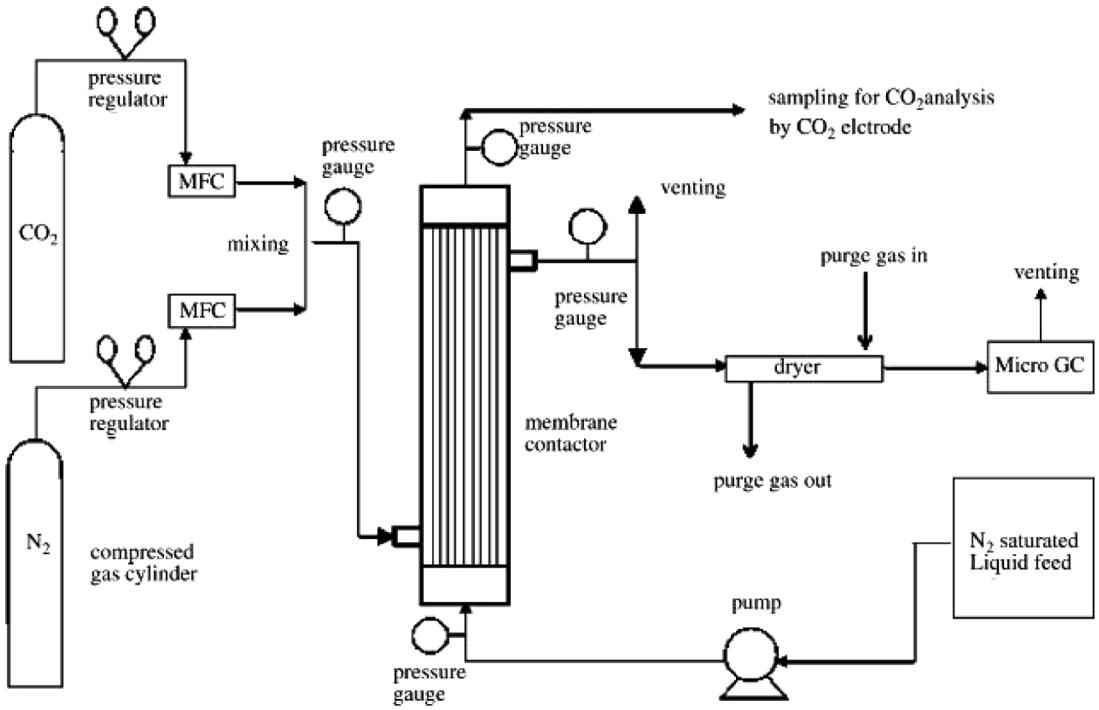

FIG. 10. Zhang et al.'s experimental setup for CO_2 absorption in a membrane contactor (24).

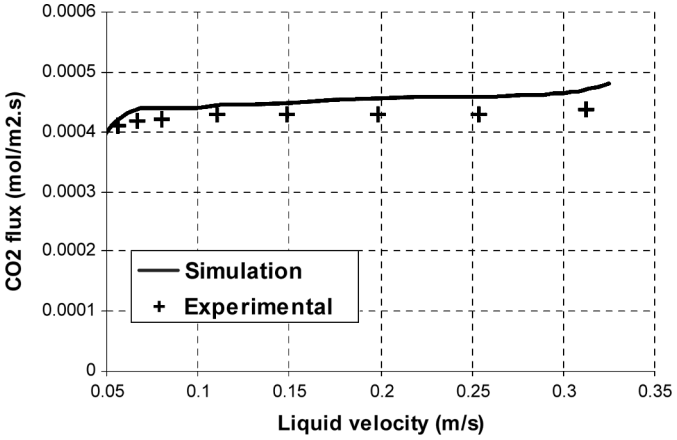

FIG. 11. Comparison between the calculated flux of CO_2 absorption obtained through simulation and the experimental data reported by Zhang et al. (24). Inlet gas velocity = 0.041 m/s; feed gas: 20/80 CO_2/N_2 mixture; absorbent: aqueous solution of 2 M DEA.

flow rate at the inlet and outlet of the membrane contactor are the same. This is a good assumption for low mass transfer fluxes because the gas flow rate does not change much. As the liquid velocity increases, the mass transfer of CO_2 increases and the gas flow rate decreases. This causes an increasing deviation between the simulation results and the experimental data.

CONCLUSIONS

Physical and chemical absorption of carbon dioxide into water and DEA solutions through hollow-fiber membrane contactors was studied. A mass transfer model was developed to describe the absorption of CO_2 through the membrane contactor. The model was based on the conservation equations for three sections of the contactor, i.e., shell, membrane, and tube. The finite element method was employed to solve the model equations. The effect of contactor operating parameters including liquid and gas flow rates as well as membrane physical properties including porosity-to-tortuosity ratio and inner diameter of the hollow fibers on the removal of CO_2 was investigated.

The simulation results were compared with the experimental data from literature obtained for a Celgard MiniModule. The comparison reveals a good agreement among the model predictions and the experimental data for flux of CO_2 absorption at different liquid velocities. The model predicts a better absorption capability of CO_2 by aqueous solution of DEA due to the incorporation of a term in the mass transfer equations which considers chemical reaction between CO_2 and DEA. The simulation results indicated that the removal of CO_2 is increased with either increasing the liquid velocity or decreasing the gas velocity in the contactor. The model predictions also reveal that the removal of CO_2 increases with either of increasing the porosity/tortuosity ratio and decreasing the inner diameter of the fibers.

The results of this work indicate that the proposed mass transfer model is capable of predicting the performance of hollow-fiber membrane contactors for gas separation processes. The proposed simulation can also take into account complex chemical reaction schemes. The developed model thus can be used to predict the mass transfer performance of the hollow-fiber membrane contactors for other reactive as well as non-reactive systems. Eventually, the proposed mass transfer model provides a preliminary design tool for multi-component membrane gas absorption processes.

NOMENCLATURE

C_0	CO_2 concentration at inlet (mol/m^3)
C	concentration (mol/m^3)
$C_{CO_2\text{-}inlet}$	CO_2 concentration at inlet (mol/m^3)
$C_{CO_2\text{-}membrane}$	CO_2 concentration in the membrane (mol/m^3)
$C_{CO_2\text{-}shell}$	CO_2 concentration in the shell (mol/m^3)
$C_{CO_2\text{-}tube}$	CO_2 concentration in the tube (mol/m^3)
C_i	concentration of species i (mol/m^3)
$C_{\text{i-}tube}$	concentration of species i in the tube (mol/m^3)
C_{int}	concentration of amine in the liquid phase at inlet (mol/m^3)
C_{in}	CO_2 volumetric concentration in the gas phase at the inlet (mol/m^3)
C_{out}	CO_2 volumetric concentration in the gas phase at the outlet (mol/m^3)
D	diffusion coefficient (m^2/s)
$D_{CO_2\text{-}membrane}$	diffusion coefficient of CO_2 in the membrane (m^2/s)
$D_{CO_2\text{-}tube}$	diffusion coefficient of CO_2 in the tube (m^2/s)
$D_{\text{i-}tube}$	diffusion coefficient of species i in the tube (m^2/s)
J_{CO_2}	flux of CO_2 ($mol/(m^2s)$)
k	reaction rate coefficient of CO_2 with DEA or OH^- ($m^3/mol \cdot s$)
L	length of the fiber (m)
m	physical solubility
n	number of fibers
P	pressure (Pa)
Q_{in}	gas flow rate at the inlet (m^3/s)
Q_{out}	gas flow rate at the outlet (m^3/s)
Q_g	gas flow rate in the contactor (m^3/s)
Q_l	liquid flow rate in the contactor (m^3/s)
R	Module radius (m)
r	radial coordinate (m)
R_i	inner tube radius (m)
R_o	outer tube radius (m)
R_e	inner shell radius (m)
$\Re_i$	overall reaction rate of species i ($mol/m^3 \cdot s$)

S	gas-liquid interfacial area (m^2)
T	Temperature (K)
U_g	gas velocity (m/s)
U_l	liquid velocity (m/s)
$\overline{V}$	average velocity (m/s)
V_z	velocity in the module (m/s)
$V_{z\text{-shell}}$	velocity in the shell (m/s)
$V_{z\text{-tube}}$	velocity in the tube (m/s)
z	axial distance (m)

Greek Symbols

ϕ	module volume fraction
μ	viscosity ($pa \cdot s$)
ρ	density (kg/m^3)
τ	tortuosity factor
ν	kinematics viscosity (m^2/s)

REFERENCES

1. Herzog, H.; Eliasson, B.; Kaarstad, O. (2000) Capturing greenhouse gases. *Sci. Am.*, 182: 72–79.
2. Desideri, U.; Paolucci, A. (1999) Performance modeling of a carbon dioxide removal system for power plants. *Energy Convers. Manage.*, 40: 1899–1915.
3. Herzog, H. (2001) What future for carbon capture and sequestration? *ES&T*, 35 (7): 148A–153A.
4. Gabelman, A.; Hwang, S.T. (1999) Hollow fiber membrane contactors. *J. Membrane Sci.*, 159: 61–106.
5. Bocquet, S.; Romero, J.; Sanchez, J.; Rios, G.M. (2007) Membrane contactors for the extraction process with subcritical carbon dioxide or propane: Simulation of the influence of operating parameters. *J. Supercrit. Fluids*, 41: 246–256.
6. Wang, K.L.; Cussler, E.L. (1993) Baffled membrane modules made with hollow fiber fabric. *J. Membrane Sci.*, 85: 265–278.
7. Gabelman, A.; Hwang, S.T.; Krantz, W.B. (2005) Dense gas extraction using a hollow fiber membrane contactor: Experimental results versus model predictions. *J. Membrane Sci.*, 257: 11–36.
8. Qi, Z.; Cussler, E.L. (1985) Microporous hollow fibers for gas absorption. *J. Membrane Sci.*, 23: 321–345.
9. Kreulen, H.; Smolders, C.A.; Versteeg, G.F.; Van Swaaij, W.P.M. (1993) Microporous hollow fiber membrane modules. *Ind. Eng. Chem. Res.*, 32: 674–684.
10. Falk-Pederson, O.; Dannstrom, H. (1997) Separation of carbon dioxide from offshore gas turbine exhaust. *Energy Convers. Manage.*, 38: S81–S86.
11. Kreulen, H.; Smolders, C.A.; Versteeg, G.F.; Van Swaaij, W.P.M. (1993) Microporous hollow fiber membrane modules as gas–liquid contactors. 2. Mass transfer with chemical reaction. *J. Membrane Sci.*, 78 (3): 217–238.
12. Kumar, P.S.; Hogendoorn, J.A.; Feron, P.H.M.; Versteeg, G.F. (2002) New absorption liquids for the removal of CO_2 from dilute gas streams using membrane contactors. *Chem. Eng. Sci.*, 57: 1639–1651.
13. Karror, S.; Sirkar, K.K. (1993) Gas absorption studies in microporous hollow fiber membrane modules. *Ind. Eng. Chem. Res.*, 32: 674–684.
14. Dindore, V.Y.; Brilman, D.W.F.; Feron, P.H.M.; Versteeg, G.F. (2004) CO_2 absorption at elevated pressures using a hollow fiber membrane contactor. *J. Membrane Sci.*, 235: 99–109.
15. Kim, Y.S.; Yang, S.M. (2000) Absorption of carbon dioxide through hollow fiber membranes using various aqueous absorbents. *Sep. Purif. Tech.*, 21: 101–109.
16. Al-Marzouqi, M.H.; El-Naas, M.H.; Marzouk, S.A.M.; Al-Zarooni, M.A.; Abdullatif, N.; Faiz, R. (2008) Modeling of CO_2 absorption in membrane contactors. *Sep. Purif. Tech.*, 59: 286–293.
17. Shirazian, S.; Moghadassi, A.; Moradi, S. (2009) Numerical simulation of mass transfer in gas-liquid hollow fiber membrane contactors for laminar flow conditions. *Simulat. Modell. Pract. Theory*, 17: 708–718.
18. Twarowska-Schmidt, K.; Wlochowicz, A. (1997) Melt-spun asymmetric poly (4-methyl- 1-pentene) hollow fiber membranes. *J. Membrane Sci.*, 137: 55–61.
19. Shavit, U.; Bar-Yosef, G.; Rosenzweig, R.; Assouline, S. (2002) Modified Brinkman equation for a free flow problem at the interface of porous surfaces: The Cantor–Taylor brush configuration case. *Water Resour. Res.*, 38 (12): 1320–1334.
20. Shavit, U.; Rosenzweig, R.; Assouline, S. (2004) Free flow at the interface of porous surfaces: A generalization of the Taylor brush configuration. *Transport. Porous Med.*, 54: 345–360.
21. Abdullah, N.S.; Das, D.B.; Ye, H.; Cui, Z.F. (2006) 3D bone tissue growth in hollow fiber membrane bioreactor: Implications of various process parameters on tissue nutrition. *Int. J. Artificial Organs.*, 29: 841–851.
22. Ye, H.; Das, D.B.; Triffitt, J.T.; Cui, Z. (2006) Modelling nutrient transport in hollow fiber membrane bioreactors for growing three-dimensional bone tissue. *J. Membrane Sci.*, 272 (1–2): 169–178.
23. Abdullah, N.S.; Das, D.B. (2007) Modelling nutrient transport in hollow fiber membrane bioreactor for growing bone tissue with consideration of multi-component interactions. *Chem. Eng. Sci.*, 62: 5821–5839.
24. Zhang, H.; Wang, R.; Tee Liang, D.; Hwa Tay, J. (2006) Modeling and experimental study of CO_2 absorption in a hollow fiber membrane contactor. *J. Membrane Sci.*, 279: 301–310.
25. Bird, R.B.; Stewart, W.E.; Lightfoot, E.N. (1960) *Transport Phenomena*; John Wiley & Sons: New York, USA, 1960.
26. Happel, J. (1959) Viscous flow relative to arrays of cylinders. *AIChE J.*, 5: 174–177.
27. Caplow, M. (1968) Kinetics of carbamate formation and breakdown. *J. Am. Chem. Soc.*, 90: 6705–6803.
28. Danckwerts, P.V. (1979) The reaction of CO_2 with ethanolamines. *Chem. Eng. Sci.*, 34: 443–446.
29. Blauwhoff, P.M.M.; Versteeg, G.F.; van Swaaij, W.P.M. (1984) A study on the reaction between CO_2 and alkanolamines in aqueous solutions. *Chem. Eng. Sci.*, 39: 207–235.
30. Versteeg, G.F.; van Swaaij, W.P.M. (1988) On the kinectics between CO_2 and alkanolamines both in aqueous and non-aqueous solutions. I. Primary and secondary amines. *Chem. Eng. Sci.*, 43: 573–585.
31. Versteeg, G.F.; Oyevaar, M.H. (1989) The reaction between CO_2 and diethanolamine at 298 K. *Chem. Eng. Sci.*, 44: 1264–1268.
32. Bosch, H.; Versteeg, G.F.; van Swaaij, W.P.M. (1990) Kinetics of the reaction of CO_2 with the sterically hindered amine 2-amino-2-methylpropanol at 298 K. *Chem. Eng. Sci.*, 45: 1167–1173.
33. Little, R.J.; Versteeg, G.F.; van Swaaij, W.P.M. (1992) Kinetics of CO_2 with primary and secondary amines in aqueous solutions. II. Influence of temperature on zwitterions formation and deprotonation rates. *Chem. Eng. Sci.*, 47: 2037–2045.
34. Xu, S.; Wang, Y.W.; Otto, F.D.; Mather, A.E. (1996) Kinetics of the reaction of carbon dioxide with 2-amino-2-methyl-1-propanol solutions. *Chem. Eng. Sci.*, 51: 841–850.